# Control of the Average Synaptic Strength in a Neural Mass Model Corresponding with Epileptic Activity

Stephanie Ogrey, Sana Khan, Keli Wang, Serena Tang, Jorge Villazon

*Abstract* - **Epilepsy is a neurological disorder in the central nervous system in which irregular brain activity results in the onset of unprovoked seizures; this abnormal activity is commonly linked to an increase in excitatory activity and a decrease in inhibitory activity in the synapses of neuron connections [1]. While it is the third most common neurological disorder, preceded only by Alzheimer's disease and stroke [2], little is known about its causes and the most effective methods of treatment. Due to its dynamical nature at the system level, computational models are regularly used to study this disorder, as well as many other disorders of the nervous system. In particular, Neural Mass Models are often used to model the interaction between coupled excitatory and inhibitory neurons, particularly to create and analyze waveforms similar to an electroencephalogram signal (EEG). In this work, the Jensen-Ritt Neural Mass Model (JR-NMM) was used to model both typical alpha wave patterns in a healthy patient along with epileptic behavior. Through creating block diagrams in Simulink, finding the transfer function for the linearized system and performing a sensitivity analysis to identify specific control parameters, it was possible to analyze how different combinations of proportional, integral, and derivative control parameters can affect the pathophysiological system response and have a positive clinical impact.**

## I. INTRODUCTION

Epilepsy is an alarmingly common neurological disorder, affecting around 50 million people worldwide [2]. Patients with epilepsy are victim to recurring seizures and other fluctuations in global brain activity, which can have adverse, and sometimes deadly outcomes. The onset of epileptic seizures is attributed to abnormalities in neuronal interactions and properties [3]; these abnormalities are often linked to hyperexcitability and hyper synchronization of neurons. Hyper-excitability occurs when there is an increased likelihood of neural networks being activated, and hyper synchronization can be thought of as high magnitude neuronal oscillations. An EEG of a patient before and after the onset of a seizure can be found in Appendix A. Figure 1; from this figure, it is shown that there are higher magnitude and higher frequency oscillations during a seizure than there are before, as measured in patients with epilepsy. This is consistent with the expected behavior under the conditions of hyperexcitability and hyper synchronization of neural networks; these conditions can result in various motor, sensory, cognitive, or behavioral symptoms [3]. Common treatment for this disorder includes antiepileptic medication, which can have strong side effects. An alternative solution, which has been gaining popularity, is deep brain stimulation (DBS) involving closed-loop control using PID-type controllers [1].

The Jensin-Ritt Neural Mass Model (JR-NMM) can be used to model epilepsy as an imbalance between excitatory and inhibitory neuron activity. A simple depiction of the neural mass model of a cortical unit can be found in Appendix A. Figure 2.

The interactions between a main population of pyramidal neurons and inhibitory and excitatory interneurons are depicted in Appendix A. Figure 2. These interactions between populations of neurons result in alpha waves, which can be measured via an EEG to show brain activity. When excitation is stronger than inhibition, this leads to instability which can manifest itself as epileptic seizures in a patient. Sigmoid functions can be used in the model to ensure that the output must be smaller than the sigmoid saturation value. Since excitation is faster than inhibition, excitation first reaches saturation, and then the inhibitory behavior takes over. This cycle repeats in a periodic manner which results in an output of epileptic spikes.

## II. DESIGN

### A. Assumptions

In order to simplify the JR-NNM and to allow us to recreate the model in Simulink, several assumptions were made. For the closed loop model, it was assumed that there is no measurement error for the local field potential of the neural mass, $y(t)$, such that we can use:

$$e(t) = y(t)_{target} - y(t) \quad (1)$$

Additionally, it was assumed that the excitatory input, $p(t)$, can be modeled with the band-limited white noise block provided in Simulink, which can accurately replicate the Gaussian white noise used in literature. Finally, it was also assumed that the transformation of the average potential of the population to the average rate of action potential fired by neurons is instantaneous and can be described by the sigmoid function.

### B. Jensin-Ritt Neural Mass Model

As mentioned previously, the Jensin-Ritt Neural Mass Model was used to model neuronal activity; it can be mathematically written as the following six-dimensional first order ODE system [4]:

$$\dot{x}_0(t) = x_3(t) \quad (2)$$

$$\dot{x}_1(t) = x_4(t) \quad (3)$$

$$\dot{x}_2(t) = x_5(t) \quad (4)$$

$$\dot{x}_3(t) = AaSigm\big(x_1(t) - x_2(t)\big) - 2ax_3(t) - a^2x_0(t) \quad (5)$$

$$\dot{x}_4(t) = Aa\big[p(t) + C_2Sigm\big(C_1x_0(t)\big)\big] - 2ax_4(t) - a^2x_1(t) \quad (6)$$

$$\dot{x}_5(t) = BbC_4Sigm\big(C_3x_0(t)\big) - 2bx_5(t) - b^2x_2(t) \quad (7)$$

The main neural population consists of three subpopulations: the main subpopulation, the excitatory feedback subpopulation, and the inhibitory feedback population. The main subpopulation can be described with a nonlinear static function:

$$S(v) = 2e_0/[1 + e^{r(v_0 - v)}] \quad (8)$$

, where $2e_0$ is the maximum firing rate, $v_0$ is the post-synaptic potential corresponding to a firing rate of $e_0$, $r$ is the steepness of the sigmoid function, and $v$ is the average presynaptic membrane potential. The excitatory and the inhibitory feedback subpopulation can be described by linear dynamic functions, $h_e(t)$ and $h_i(t)$, respectively:

$$h_e(t) = \frac{H_e}{\tau_e} t e^{-\frac{t}{\tau_e}} \quad (9)$$

$$h_i(t) = \frac{H_i}{\tau_i} t e^{\frac{-t}{\tau_i}} \quad (10)$$

, where $H_e$ and $H_i$ are the excitatory and inhibitory average synaptic gain, respectively, and $\tau_e$and $\tau_i$are lumped representations of the membrane time constants.

Additionally, in order to take advantage of the linear system theory, a linear approximation of the neural population model was derived around its equilibrium point; therefore, the nonlinear sigmoid function was linearized around the equilibrium point $v = v_0$:

$$Ks = S'(v)|_{v=v_0} = \frac{2e_0 r e^{r(v_0 - v)}}{[1+e^{r(v_0-v)}]^2}|_{v=v_0} = \frac{e_0 r}{2} \quad (11)$$

, where Ks is the slope of $S(v_o)$ at the equilibrium point and referred to as the sigmoid gain. The linear approximation of the neural population model, $G_{NPM}$, can be described with the following transfer function:

$$G_{NPM} = \frac{Y(s)}{P(s)} = \frac{G_e(s)}{1+K_s{}^2 G_e(s)[C_3 C_4 G_i(s) - C_1 C_2 G_e(s)]} \quad (12)$$

$$G_e(s) = \frac{H_e \tau_e}{(\tau_e s+1)^2} \quad (13)$$

$$G_i(s) = \frac{H_i \tau_i}{(\tau_i s+1)^2} \quad (14)$$

, where $G_e(s)$and $G_i(s)$are the laplace transform function of $h_e(t)$ and $h_i(t)$, respectively.

### C. *Baseline Jensen-Ritt Neural Mass Model*

In the healthy, baseline JR-NMM, its simulated model appears as a normal EEG reading. The value of each of the contents can be found in Appendix A. Table 1., where $H_e$ and $H_i$ were used in the baseline mode [4].

Based on these values, the block diagram of the system was recreated and shown in Figure 1.

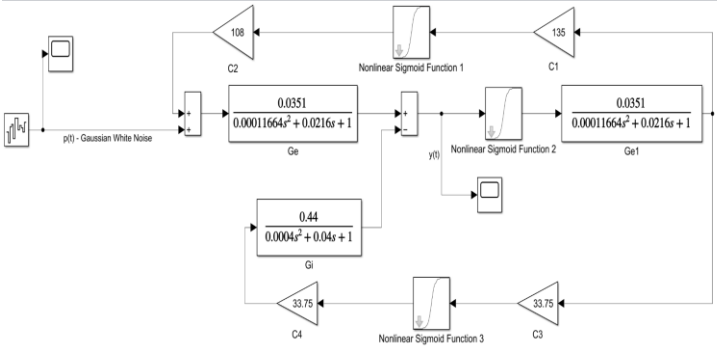


**Figure 1.** Simulink block diagram of baseline JR-NMM.

The simulated output of this block diagram is shown in Figure 2 and appears to resemble that of an EEG.

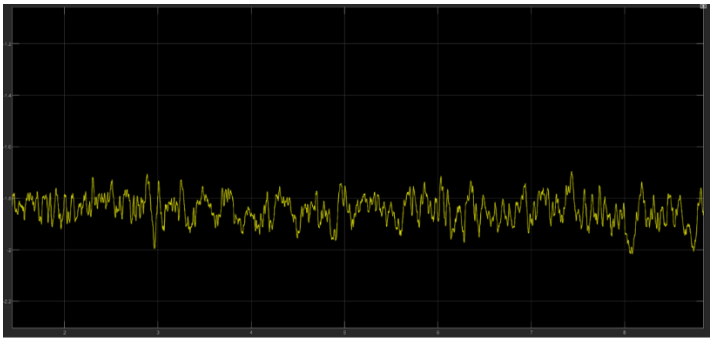

**Figure 2.** Simulated output of the baseline JR-NMM.

### D. *Modified Epileptic Parameters*

The JR-NMM can be modified to produce waveforms similar to those of an EEG recording during an epileptic seizure. This is done by changing parameters from the baseline model to represent the activity of excitatory and inhibitory neurons. In this, we first consider the case of hyper-excitatory. The synaptic gain from excitatory neurons, $H_e$, is increased to simulate increased excitatory activity; for this, the value of $H_e$ is increased to $H_{e_d} = 7$ mV. However, all other parameters, including the time constant of the excitatory postsynaptic potential (EPSP) $T_e$, are unchanged. It is thought that the increased synaptic gain is most likely due to an increase in extracellular concentration of the neurotransmitter glutamate in the brain.

Furthermore, we consider the second case of low inhibition; for this, the synaptic gain from the inhibitory neurons, $H_i$, is decreased to simulate decreased inhibitory activity. In this case, the value of $H_i$ was decreased to $H_{i_d} = 17$ mV; similar to the hyper-excitatory model, the remaining parameters remained unchanged. Additionally, the decreased inhibitory gain is believed to be due to a decrease in concentration of γ-aminobutyric acid (GABA), an inhibitory neurotransmitter.

## III. ANALYSIS

### A. *Baseline Jensen-Ritt Neural Mass Model*

From the transfer function of the baseline JR-NNM, Equation 12, its poles and zeros can give information about the stability of the system. By setting the numerator to zero, its zeros were found to be $Z_1 = -92.59$, $Z_2 = -92.59$, $Z_3 = -50$, and $Z_4 = -50$. Additionally, by setting the denominator to zero, its poles were found to be $P_1 = -244.6$, $P_2 = -99 + 150i$, $P_3 = -99 - 150i$, $P_4 = -64.83$, $P_5 = 25.7$, and $P_6 = 11.39$. Due to the presence of the two positive, real poles, the baseline JR NNM was found to be unstable. Furthermore, from the transfer function, the bode plot was able to be constructed, shown in Figure 3.

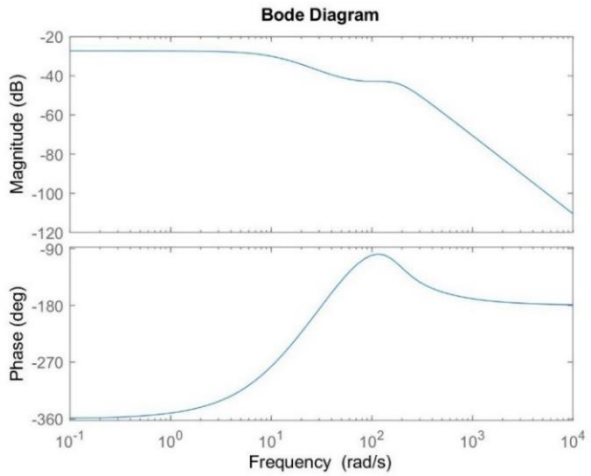


**Figure 3.** Bode Diagram of the baseline JR-NMM.

*B. Diseased Jensen-Ritt Neural Mass Model*

In order to understand the system response of the diseased state of the JR-NMM, the transfer function of each case was found and analyzed.

In the case of hyper-excitation, the transfer function of the system was found to be:

$$H(s) = \frac{(3.53\times10^{-9})s^4+(1.006\times10^{-6})s^3+0.000104s^2+0.004657s+0.0756}{(5.44\times10^{-5})s^6+(2.56\times10^{-9})s^5+(4.95\times10^{-7})s^4+(5.03\times10^{-5})s^3-0.0113s^2-1.149s-21.27} \quad (15)$$

Based on this transfer function, the bode diagram was plotted in Figure 4.

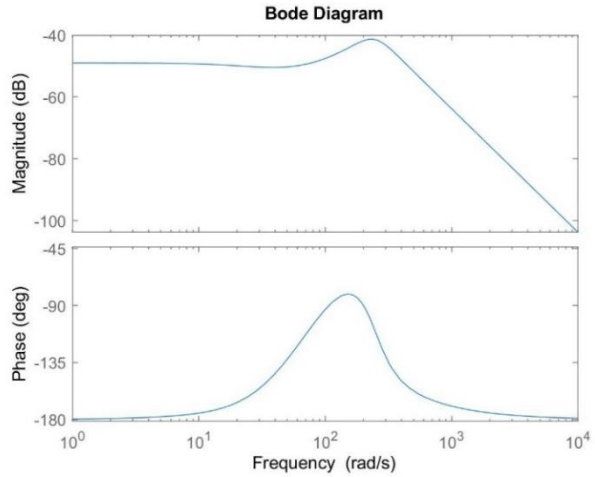


**Figure 4.** Bode Diagram of the hyper excited JR-NMM.

Additionally, the zeros of Equation 15 were found to be $Z_1 = -92.59$, $Z_2 = -92.59$, $Z_3 = -50$, and $Z_4 = -50$. Additionally, the poles of this system were found to be $P_1 = -320.9$, $P_2 = -95.6 + 226.8i$, $P_3 = -95.6 - 226.8i$, $P_4 = 128.5$, $P_5 = -61.4$, and $P_6 = -25.5$; due to the presence of positive, real pole $P_4$, the case of hyper excitation is unstable.

This system was also simulated in Simulink; its simulation is shown in Figure 5.

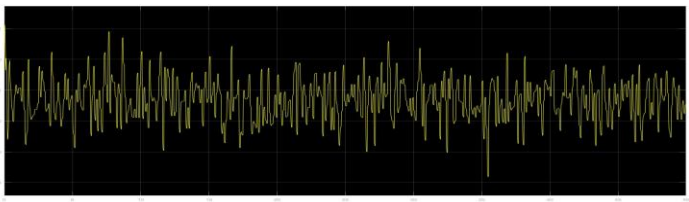

**Figure 5.** Simulated output of the hyper excited JR-NMM.

Based on this result, the simulated output has a higher amplitude and oscillation frequency, as is expected from an epileptic EEG wave.

In the case of low inhibition, the transfer function of the system was found to be:

$$H(s) = \frac{(1.64\times10^{-9})s^4+(4.67\times10^{-7})s^3+(4.85\times10^{-5})s^2+0.002162s+0.0351}{(5.44\times10^{-12})s^6+(2.56\times10^{-9})s^5+(4.95\times10^{-7})s^4+(5.03\times10^{-5})s^3+\left(8.41\times10^{-5}\right)s^2-0.125s-1.141} \quad (16)$$

Based on this transfer function, the bode diagram was plotted in Figure 6.

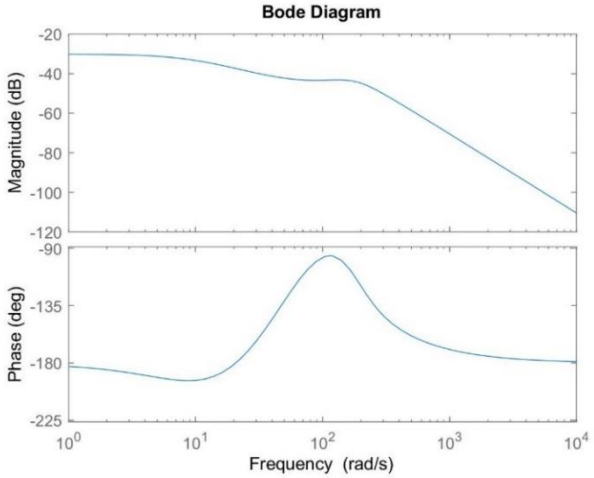


**Figure 6.** Bode Diagram of the low inhibition JR-NMM.

Furthermore, the zeros of Equation 16 matched those of Equation 15. The poles of this system were found to be $P_1 = -246.4$, $P_2 = -97.34 + 152i$, $P_3 = -97.34 - 152i$, $P_4 = -63.62$, $P_5 = 43.68$, and $P_6 = -9.37$; again, due to the presence of positive, real pole $P_5$, the case of low inhibition is also unstable. This system was also simulated in Simulink; its simulation is shown in Figure 7.

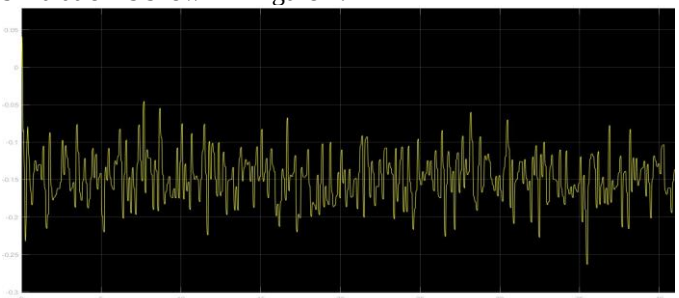

**Figure 7.** Simulated output of the low inhibition JR-NMM.

This simulation has results similar to that hyper-excitation state of the JR NMM such that it is higher in amplitude and oscillation frequency than that of the baseline model.

*C. Adding PI Control*

In order to help stabilize the JR-NNM, a proportional integral (PI) controller was added to the NNM in the hyper-excitation and low-inhibition state. In the first case of hyper-excitation, a proportional controller value of 310 and an integral controller of 2 was added based on literature [1]; the controller transfer function is given by:

$$F(s) = 310s + 2 \quad (17)$$

Therefore, from the NMM and controller transfer functions, the open loop transfer function is the product of the two; the open loop transfer function for case 1 is given by:

$$OL(s) = \frac{(1.09\times10^{-6})s^5+0.000312s^4+0.0324s^3+1.44s^2+23.45s+0.151}{(5.44\times10^{-12})s^7+(2.56\times10^{-9})s^6+(4.95\times10^{-7})s^5+(5.03\times10^{-5})s^4+0.0113s^3-1.15s^2-21.27s} \quad (18)$$

From this, the bode diagram was plotted as shown in Figure 8.

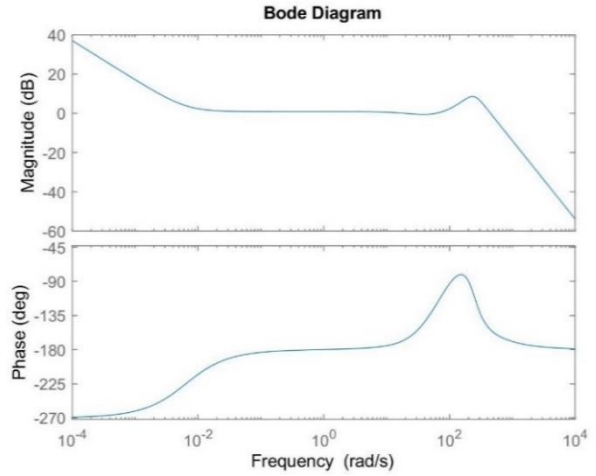


**Figure 8.** Open loop bode diagram of the hyper-excitation state of the JR-NNM with PI control.

Based on the bode diagram of the open loop response, it will give information about the closed loop response, such as its stability. From Figure 8, the phase margins were determined to be 12.2 degree, 57.9 degrees, and 26 degrees; therefore, as none of the phase margins are 0, the closed loop system response will be stable. In order to confirm the closed loop system response, the closed loop transfer function and bode diagram were also found. The closed loop function can be found by:

$$CL(s) = OL(s)/(1 + OL(s)) \quad (19)$$

From the closed loop transfer function of this system, the bode diagram of the closed loop system was found and shown in Appendix B. Figure 3.

From the transfer function, the poles of this system were found to be $P_1 = -92.94 - 461.72i$, $P_2 = -92.94 + 461.72i$, $P_3 = -206.79$, $P_4 = -61.65$, $P_5 = 7.995 + 8.7i$, $P_6 = 7.995 - 8.7i$, and $P_7 = -0.07$; therefore, the closed loop system response is stable as all the poles are negative, just as the open loop system predicted.

For case 2, a proportional controller of 90 and an integral control of 2 was used; the controller transfer function is given by:

$$F(s) = 90s + 2 \quad (20)$$

Therefore, the open loop transfer function for case 2 was found to be:

$$OL(s) = \frac{(1.474\times10^{-7})s^5+(4.204\times10^{-5})s^4+0.004362s^3+0.1947s^2+3.163s+0.0702}{(5.44\times10^{-12})s^7+(2.56\times10^{-9})s^6+(4.95\times10^{-7})s^5+(5.03\times10^{-5})s^4+(8.41\times10^{-5})s^3-0.125s^2-1.14s} \quad (21)$$

From this, the bode diagram was plotted as shown in Figure 9.

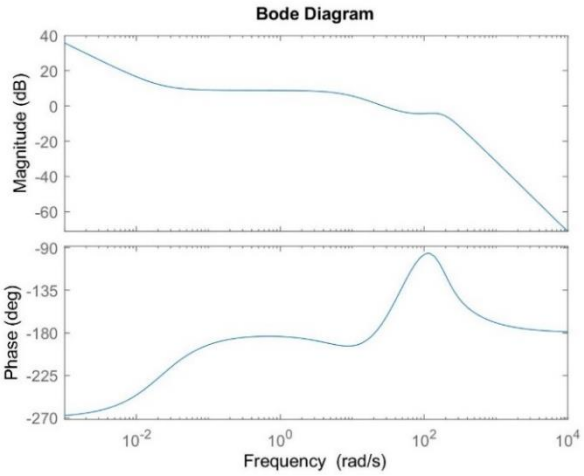


**Figure 9.** Open loop bode diagram of the low-inhibition state of the JR-NNM with PI control.

From Figure 9, the phase margin was determined to be 11.4 degrees; therefore, since the phase margin is not 0, the closed loop system response will be stable. In order to confirm the closed loop system response, the closed loop transfer function and bode diagram were also found. From the closed loop transfer function, the bode diagram of the system was found and is shown in Appendix B. Figure 4.

Furthermore, from the transfer function, the poles of this system were found to be $P_1 = -95.17 - 200i$, $P_2 = -95.17 + 200i$, $P_3 = -210.51$, $P_4 = -63.78$, $P_5 = -2.85 + 23.53i$, $P_6 = -2.85 - 23.53i$, and $P_7 = -0.035$; as all the poles of this system are negative, the closed loop system loop is stable.

*D. Adding PID Control*

To further help stabilize the system, a PID controller was used. In both cases of hyper-excitation and low inhibition, the same PI controls from the above section and a derivative controller of 50 was used; the transfer function of the PID controllers are:

$$F(s) = 50s^2 + 310s + 2 \quad (22)$$

$$F(s) = 50s^2 + 90s + 2 \quad (23)$$

for the hyper-excitation and low-inhibition state, respectively. For the first case of hyper-excitation, the open loop transfer function becomes:

$$OL(s) = \frac{(1.76\times10^{-6})s^5+(5.14\times10^{-5})s^4+0.2652s^3+5.224s^2+23.45s+0.151}{(5.44\times10^{-12})s^7+(2.56\times10^{-9})s^6+(4.95\times10^{-7})s^5+(5.03\times10^{-5})s^4+0.0113s^3-1.15s^2-21.27s} \quad (24)$$

; the resulting bode diagram is shown in Figure 10.

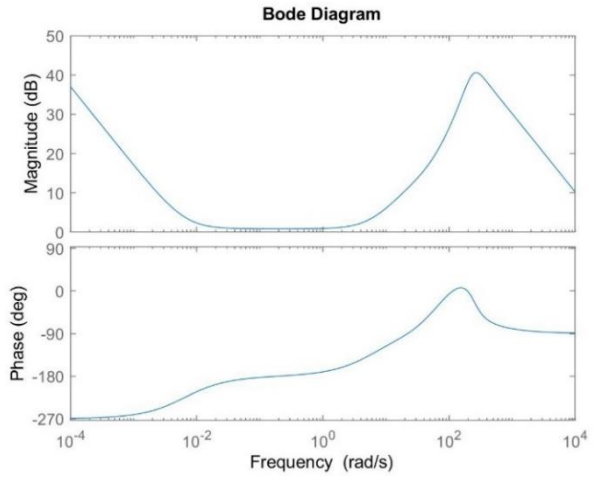


**Figure 10.** Open loop bode diagram of the hyper-excitation state of the JR-NNM with PID control.

From Figure 10, the phase margin was determined to be 90.3 degrees; therefore, the closed loop system response will be stable. In order to confirm the closed loop system response, the closed loop transfer function and bode diagram were also found; the bode diagram of the closed loop system was found and is shown in Appendix C. Figure 5.

Furthermore, from the transfer function, the poles of this system were found to be $P_1 = -32586.2$, $P_2 = -98.12 + 30.5i$, $P_3 = -98.12 - 30.5i$, $P_4 = -59.45$, $P_5 = -35.37$, $P_6 = -0.47$, and $P_7 = -0.08$; therefore, as all the poles are negative, the closed loop system response is stable. For the second case of low inhibition, the open loop transfer function can be written as follows:

$$OL(s) = \frac{(8.19 \times 10^{-8})s^6 + (2.35 \times 10^{-5})s^5 + 0.00247s^4 + 0.1125s^3 + 1.95s^2 + 3.163s + 0.0702}{(5.44 \times 10^{-12})s^7 + (2.56 \times 10^{-9})s^6 + (4.95 \times 10^{-7})s^5 + (5.03 \times 10^{-5})s^4 + (8.41 \times 10^{-5})s^3 - 0.125s^2 - 1.14s} \quad (25)$$

; its resulting bode diagram is depicted in Figure 11.

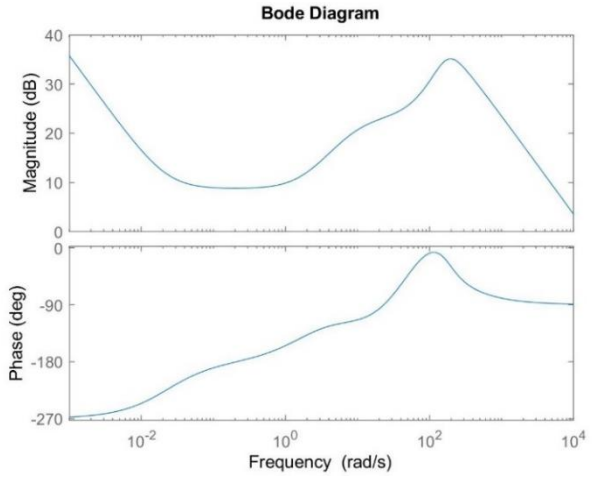


**Figure 11.** Open loop bode diagram of the low-inhibition state of the JR-NNM with PID control.

From Figure 11, the phase margin was determined to be 90.7 degrees; therefore, the closed loop system response will be stable. In order to confirm the closed loop system response, the closed loop transfer function and bode diagram were also found; the bode diagram for this system is also shown in Appendix C. Figure 6.

Furthermore, from the transfer function, the poles of this system were found to be $P_1 = -15229.1, P_2 = -95.34 - 21.18i, P_3 = -95.34 + 21.18i, P_4 = -59.84, P_5 = -35.81, P_6 = -1.12,$ and $P_7 = -0.04$; therefore, as all the poles are negative, the closed loop system response is stable.

## IV. DISCUSSION

Simulating alpha wave behavior using the JR-NMM results in simulations that resemble those shown on the EEG of a healthy, resting patient; however, these results do not exactly match those shown in literature [5]. This is likely due to the fact that these works omitted the exact noise block pulse width and amplitude parameters utilized in their respective simulations. When modifying the parameters by increasing excitatory synaptic gain and decreasing inhibitory synaptic gain, the peaks had higher amplitudes and frequency which is equivalent to recorded seizures on an EEG. Similar results can be generated by modifying the time constant values utilized in the model. For example, increasing the value of the average time constant of the inhibitory postsynaptic potential is another method for modelling decreased inhibitory behavior.

While the JR- NMM itself and its baseline constants are highly accepted and referenced in the fields of neuroscience and neuroengineering, the specific modified inhibitory and excitatory gain values chosen to simulate epilepsy are only found in two pieces of literature [5]; therefore, it is unclear how much thorough testing has been completed to validate the accuracy of these particular constant values. Despite the inherent estimations and limitations of mathematical models, they can be advantageous as alternatives to physiologic experimentation. In the case of epilepsy, it would be highly unethical to repeatedly trigger or induce seizures in patients to test the efficacy of different control parameters.

For future directions, it could be advantageous to test the proportional, derivative, and integral control schemes defined on this work on other neural mass models which simulate the frequency rhythms of alpha waves. An example of one such model is the Wendling Model, which builds off the JR- NMM by adding an additional inhibitory loop and corresponding constants [6]. Another further direction includes testing the developed control scheme on a pathophysiological model with slightly different altered inhibitory and excitatory gain or time constants. All in all, a control system approach to regulating symptoms of epilepsy through neural mass models has been demonstrated to be beneficial over the conventional pathophysiological approach; however, since little information is available, there is much work left to be done. Future research should focus on the refinement of this model.

## ACKNOWLEDGEMENTS

The authors would like to thank the instructional assignments for the Biosystem and Controls course, BENG 122a, that helped us throughout the quarter as well as Professor Gert Cauwenberghs for his invaluable guidance throughout the fall quarter.

## V. APPENDIX

### A. Neural Mass Model

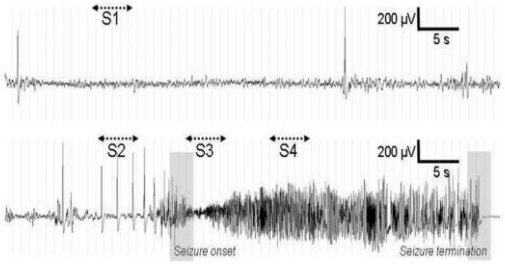


**Figure 2.** EEG before (top graph) and after (bottom graph) the onset of a seizure [3]

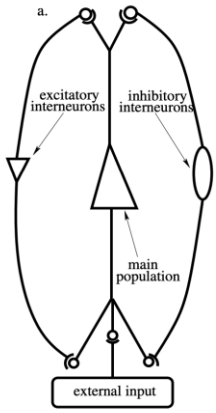


**Figure 2.** Neural Mass Model of a Cortical Unit [1]

| Constant | Description | Value |
|---|---|---|
| He | Average excitatory synaptic gain | 3.25 mV |
| $He_d$ | Increased excitatory synaptic gain in diseased state | 7 mV |
| Hi | Average inhibitory synaptic gain | 22 mV |
| $Hi_d$ | Decreased inhibitory synaptic gain in diseased state | 17 mV |
| $T_e$ | Average time constant of excitatory postsynaptic potential | 0.0108 s |
| $T_i$ | Average time constant of inhibitory postsynaptic potential | 0.02 s |
| C | Average number of synapses between excitatory and inhibitory populations | 135 |
| $C_1$ | Average number of synapses established by principal neurons on excitatory neurons | C = 135 |
| $C_2$ | Average number of synapses established by excitatory interneurons on principle neurons | 0.8C = 108 |
| $C_3$ | Average number of synapses established by principal neurons on inhibitory neurons | 0.25C = 33.75 |
| $C_4$ | Average number of synapses established by inhibitory interneurons on principle neurons | 0.25C = 33.75 |
| $v_{max}$ | Maximum neuron firing rate (maximum of sigmoid function) | 5 $s^{-1}$ |
| $v_0$ | Value at which 50% of the maximum neuron firing rate is attained | 6 mV |
| r | Slope of sigmoid function at $v_0$ | 0.56 $mV^{-1}$ |

**Table 1.** Physiological interpretation and standard values of the parameters in the JR-NMM [4]

B. Closed Loop Bode Diagrams for PI Control

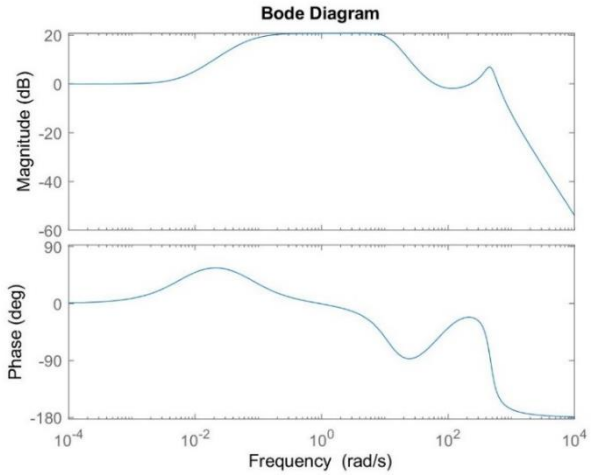


**Figure 3.** Closed loop bode diagram of the hyper-excitation state of the JR-NNM with PI control.

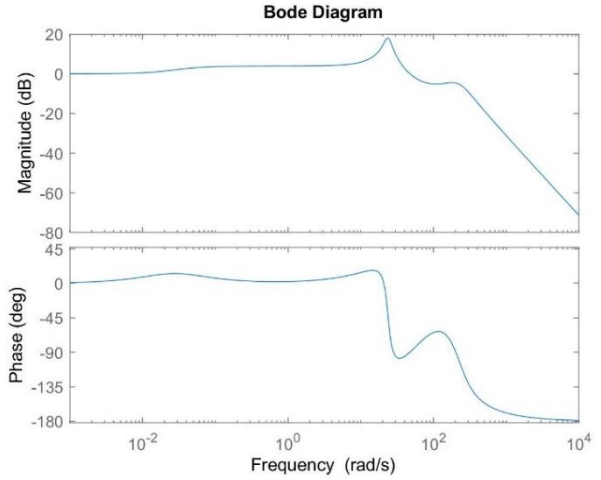


**Figure 4.** Closed loop bode diagram of the low-inhibition state of the JR-NNM with PI control.

C. Closed Loop Bode Diagrams for PID Control

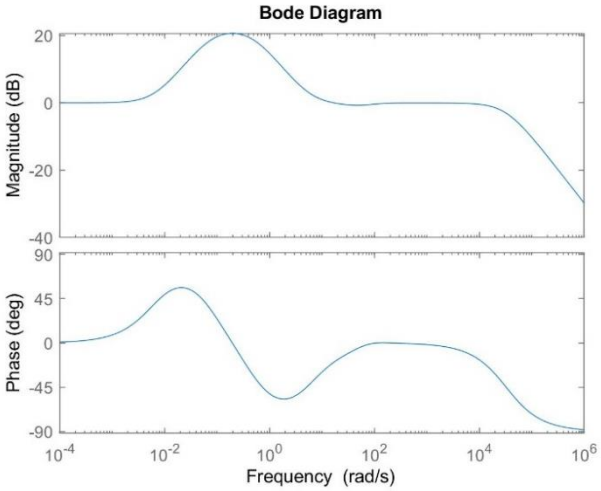


**Figure 5.** Closed loop bode diagram of the hyper excitation state of the JR-NNM with PID control.

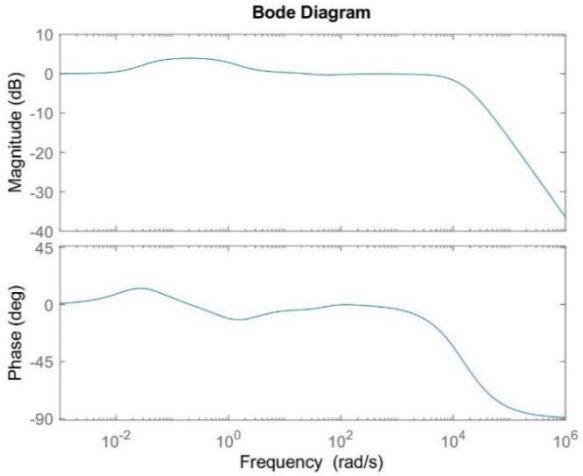


**Figure 6.** Closed loop bode diagram of the low-inhibition state of the JR-NNM with PID control.

REFERENCES

[1] Wang, J. et al. Suppressing epileptic activity in a neural mass model using a closed-loop proportional-integral controller. Sci. Rep. 6, 27344; doi: 10.1038/srep27344 (2016)

[2] Wang Jun-Song, Wang Mei-Li, Li Xiao-Li, Ernst Niebur. Closed-loop control of epileptiform activities in a neural population model using a proportional-derivative controller* . Chinese Physics B, 2015, 24(3): 038701

[3] Jonathan Touboul, Fabrice Wendling, Patrick Chauvel, Olivier Faugeras. Neural mass activity, bifurcations, and epilepsy.. Neural Computation, Massachusetts Institute of Technology Press (MIT Press), 2011, 23 (12), pp.3232-86. ff10.1162/NECO_a_00206ff. Ffinria-00592529v2

[4] Ableidinger, M., Buckwar, E., & Hinterleitner, H. (2017). A Stochastic Version of the Jansen and Rit Neural Mass Model: Analysis and Numerics. *Journal of mathematical neuroscience*, *7*(1), 8. https://doi.org/10.1186/s13408-017-0046-4

[5] Xu Y, Zhang CH, Niebur E, Wang JS. Analytically determining frequency and amplitude of spontaneous alpha oscillation in Jansen's neural mass model using the describing function method. Chin Phys B. 2018 Apr;27(4):048701. doi: 10.1088/1674-1056/27/4/048701. PMID: 34322160; PMCID: PMC8315699.

[6] Islam, S., Islam, S., & Islam, M. S. (2021). Neural mass model-based different EEG signal generation and analysis in Simulink. *Indian Journal of Signal Processing*, *1*(3), 1–7. https://doi.org/10.35940/ijsp.c1008.081321